Hox Control of Organ Size by Regulation of Morphogen Production and Mobility

Michael A. Crickmore[1] and Richard S. Mann[2]*

Selector genes modify developmental pathways to sculpt animal body parts. Although body parts differ in size, the ways in which selector genes create size differences are unknown. We have studied how the *Drosophila* Hox gene *Ultrabithorax* (*Ubx*) limits the size of the haltere, which, by the end of larval development, has ~fivefold fewer cells than the wing. We find that *Ubx* controls haltere size by restricting both the transcription and the mobility of the morphogen Decapentaplegic (Dpp). *Ubx* restricts Dpp's distribution in the haltere by increasing the amounts of the Dpp receptor, *thickveins*. Because morphogens control tissue growth in many contexts, these findings provide a potentially general mechanism for how selector genes modify organ sizes.

Changes in body part sizes have been critical for diversification and specialization of animal species during evolution. The beaks of Darwin's finches provide a famous example for how adaptation can produce variations in size and shape that allowed these birds to take advantage of specialized ecological niches and food supplies (*1*). Sizes also vary between homologous structures within an individual. For example, vertebrate digits and ribs vary in size, likely due to the activities of selector genes such as the Hox genes (*2*–*4*). Although the control of organ growth by selector genes is likely to be common in animal development (*2*, *5*, *6*), little is known about the mechanisms underlying this control.

The two flight appendages of *Drosophila melanogaster*, the wing and the haltere, provide a classic example of serially homologous structures of different sizes (Fig. 1A). Halteres, appendages used for balance during flight, are thought to have been modified from full-sized hindwings during the evolution of two-winged flies from their four-winged ancestors (*7*, *8*). All aspects of haltere development that distinguish it from a wing, including its reduced size, are under the control of the Hox gene *Ultrabithorax* (*Ubx*), which is expressed in all haltere imaginal disc cells but not in wing imaginal disc cells (*8*, *9*) (Fig. 1B). At all stages of development, haltere and wing primordia (imaginal discs) are different sizes. In the embryo, the wing primordium has about twice as many cells as the haltere primordium (*7*, *10*). By the end of larval development, the wing disc has ~five times more cells (~50,000) than the haltere disc (~10,000) (*11*) [Fig. 1B and Supporting Online Material (SOM) Text]. The wing and haltere appendages will form from the pouch region of these mature discs (fig. S1). The final step that contributes to wing and haltere size differences occurs during metamorphosis, when

[1]Department of Biological Sciences, Columbia University, New York, NY 10027, USA. [2]Department of Biochemistry and Molecular Biophysics, Columbia University, HHSC 1104, 701 West 168th Street, New York, NY 10032, USA.

*To whom correspondence should be addressed. E-mail: rsm10@columbia.edu

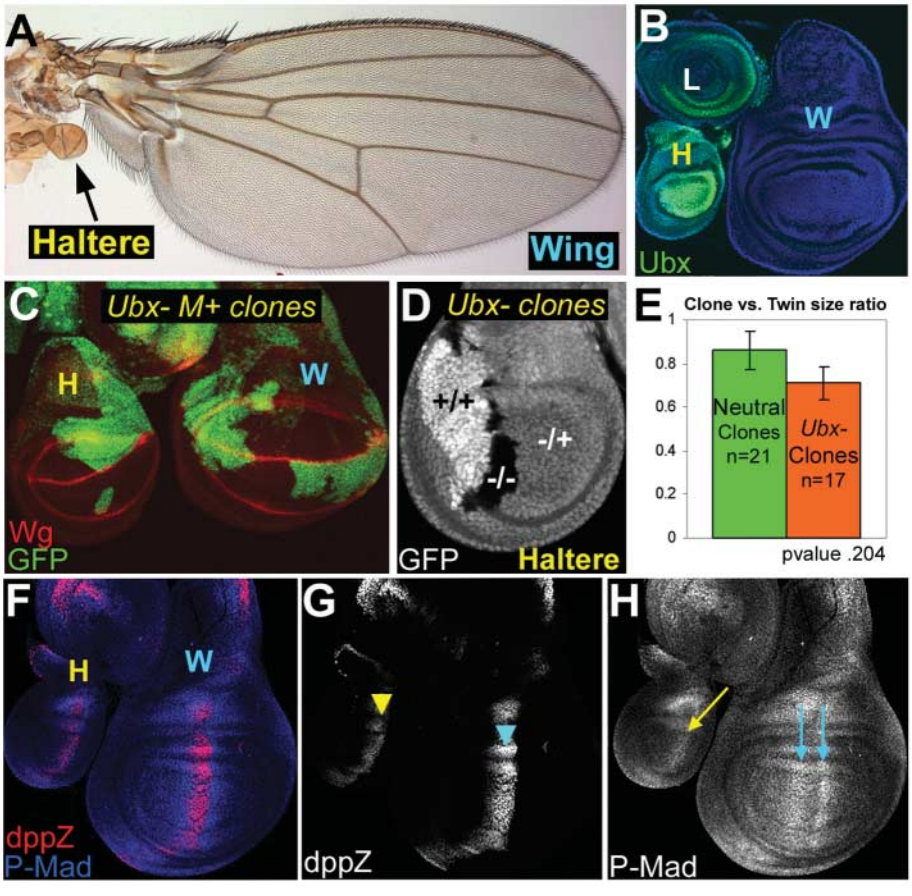

Fig. 1. Reduced Dpp production and transduction in the haltere. (**A**) Wild-type adult wing and haltere (arrow). (**B**) Third instar wing (W), haltere (H), and T3 leg (L) imaginal discs stained for Ubx (green) and a ubiquitous nuclear protein (blue). Ubx is present in all haltere disc cells but not in wing disc cells. (**C**) Removing *Ubx* activity (lack of GFP) from more than 50% of a haltere disc during larval development using the M^+ (*Minute*) technique (*13*) (SOM Text) increased its size [compare with discs in (B) and (F)]. (**D**) Isolated Ubx^- clones (black, $-/-$) were not larger than Ubx^+ twin spots (bright white, $+/+$) in a *Ubx* heterozygous haltere (gray, $-/+$). (**E**) *Ubx* mutant:twin spot and neutral:twin spot clone size ratios. Error bars indicate SEM. (**F** to **H**) Wild-type wing and haltere discs stained for *dpp-lacZ* and P-Mad patterns. In the haltere, *dpp-lacZ* was reduced (arrowheads) and overlapped with a compacted P-Mad gradient (arrows).

wing, but not haltere, cells flatten, thus increasing the surface area of the final appendage (*12*).

Nonautonomous control of haltere size by *Ubx*. To confirm that *Ubx* has a postembryonic role in limiting the size of the haltere disc, we generated Ubx^- clones midway through larval development (*13*). Haltere discs–bearing large Ubx^- clones generated at this time become much larger than wild-type discs (Fig. 1C and SOM Text). *Ubx* could limit haltere size cell-autonomously by, for example, slowing the cell cycle of haltere cells relative to wing cells. We tested this by comparing the sizes of isolated Ubx^- clones in the haltere with those of their simultaneously generated wild-type twin clones. Contrary to the prediction of a cell-autonomous function for *Ubx* in size control, *Ubx* mutant clones did not grow larger than their twins (Fig. 1, D and E), a result that is consistent with earlier experiments suggesting that wing and haltere cells have similar mitotic rates during development (*14*). Hence, *Ubx* limits the size of the haltere during larval development by modifying pathways that control organ growth cell-nonautonomously.

***Ubx* regulation of Dpp signaling.** In the fly wing, Decapentaplegic (Dpp) [a long-range morphogen of the bone morphogenetic protein (BMP) family] has been shown to promote growth (*15*–*17*). In both the wing and the haltere, Dpp is produced and secreted from a specialized stripe of cells called the AP organizer, which is induced by the juxtaposition of anterior (A) and posterior (P) compartments, two groups of cells that have separate cell lineages (*18*). The AP organizer is a stripe of A cells that are instructed to synthesize Dpp by the short-range morphogen Hedgehog (Hh) secreted from adjacent P compartment cells (*18*–*22*). Dpp has a positive role in appendage growth. When more Dpp is supplied to the wing disc, either ectopically or within the AP organizer, more cells are incorporated into the developing wing field (*22*–*24*). Conversely, mutations that reduce the amount of Dpp lead to smaller wings (fig. S3) (*25*).

A comparison of the expression patterns of Dpp pathway components in the wing and the haltere demonstrates that *Ubx* is modifying this pathway (Fig. 1, F to H, fig. S1, and SOM Text). Compared with the wing, the stripe of *dpp* expression in the haltere was reduced in both its width and intensity, as reported by a *lacZ* insertion into the *dpp* locus (*dpp-lacZ*). There was also a difference in the profile of Dpp pathway activation, as visualized by an antibody that detects P-Mad, the activated form of the Dpp pathway transcription factor Mothers against Dpp (Mad). In the wing, P-Mad staining was low in the cells that transcribe *dpp* (Fig. 1, F to H, and fig. S1) (*26*). Immediately anterior and posterior to this activity trough, P-Mad labeling peaked in intensity and then gradually decayed further from the Dpp source, revealing a bimodal activity gradient. In contrast, in the haltere intense P-Mad staining was detected only in a single stripe of cells that overlaps with Dpp-producing cells of the AP organizer (Fig. 1, F to H, and fig. S1).

Because of the coincidence between *dpp* transcription and peak P-Mad staining in the haltere, we hypothesized that Dpp might be less able to move from haltere cells that secrete this ligand. We tested this idea by generating clones of cells in both wing and haltere discs in which the *actin5c* promoter drove the expression of a green fluorescent protein (GFP)–tagged version of Dpp (Dpp:GFP) (*13*, *27*, *28*). By using an extracellular staining protocol to analyze simultaneously generated clones (*29*), we observed Dpp:GFP and P-Mad much further from producing cells in the wing than in the haltere (Fig. 2, A to D). These observations strongly suggest that, compared with the wing, Dpp's mobility—and consequently the range of Dpp pathway activation—is reduced in the haltere.

We also tested whether the decreased production of Dpp in the haltere contributes to the different pattern of pathway activation observed in this tissue compared with the wing. This is unlikely because, even in haltere discs that overexpress Dpp in its normal expression domain, peak P-Mad staining was still observed close to Dpp-expressing cells (Fig. 2, E and F) (*13*). Despite increased *dpp* expression, no P-Mad activity trough was observed in these haltere discs. Further, although they become larger, these discs remained smaller than wild-type wing discs. We conclude that the decreased Dpp production in the haltere contributes to its reduced growth, but there must be mechanisms that also limit the extent of Dpp pathway activation, even in the presence of increased Dpp production.

One way in which Dpp's activation profile can be modified is by varying the production of the type I Dpp receptor, Thickveins (Tkv) (*26*, *30*). In the wing, *tkv* expression is low within and around the source of Dpp, resulting in low Dpp signal transduction in these cells and robust Dpp diffusion (*26*, *30*, *31*) (Fig. 3, A and B, and fig. S1). Low *tkv* expression in the medial wing is due to repression by both Hh and Dpp (*26*, *30*). Accordingly, *tkv* expression is highest in lateral regions of the wing disc, where Hh and Dpp signaling are low. In contrast to the wing, *tkv* transcription and protein levels were high in all cells of the haltere (Fig. 3, A and B). Thus, the more restricted Dpp mobility and P-Mad pattern in the haltere may result from a failure to repress *tkv* medially. To test this idea, we supplied all cells of the wing disc with uniform $UAS\text{-}tkv^+$ expression, to mimic the haltere pattern (Fig.

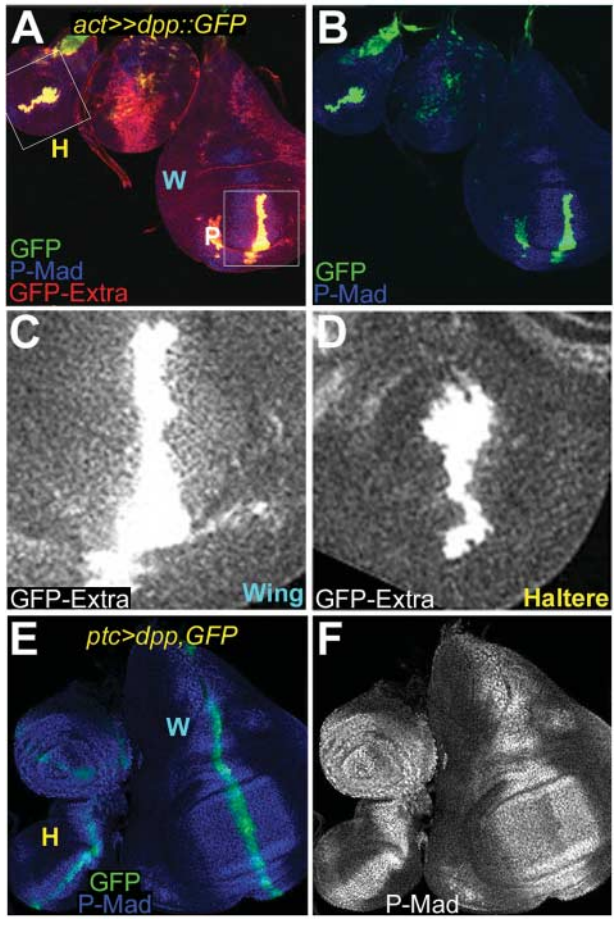

Fig. 2. Reduced Dpp mobility in the haltere. (**A** to **D**) Simultaneously generated *actin5c* promoter flp-out clones expressing *UAS-dpp::gfp* and *UAS-GFP* in the wing and haltere stained for extracellular GFP (red and white) and P-Mad (blue). The green channel shows GFP autofluorescence and marks the clone. The extracellular Dpp::GFP pattern closely correlates with the P-Mad pattern. In (C) and (D), enlarged images of the regions boxed in (A) are shown. (**E** and **F**) Overexpressing *dpp* with *ptc-Gal4* (visualized with *UAS-GFP*) increased the scale and intensity of P-Mad staining in the wing and the haltere, but the patterns remained qualitatively similar to those of wild type.

3C) (*13*). The resulting P-Mad pattern in these wing discs was very similar to that found in the wild-type haltere: The P-Mad trough was gone, and the activity gradient was compacted into a single stripe that coincides with Dpp-producing cells. Conversely, lowering the amount of Tkv in the haltere by expressing an RNA interference (RNAi) hairpin construct directed against *tkv* (*UAS-tkvRNAi*) in Dpp-producing cells induced a bimodal pattern of P-Mad staining similar to that of the wild-type wing disc (Fig. 3, D to F) (*13*). Thus, different amounts of Tkv result in qualitative differences in the P-Mad profiles of the wing and the haltere.

***tkv* expression and appendage size.** We hypothesized that the more limited pathway activation in the haltere might contribute to its smaller size. If correct, increasing *tkv* expression in the wing should reduce its size. Adult wings from flies expressing uniform *UAS-tkv*$^{+}$ were ~30% smaller than control wings; however, wing cell size remained the same (Fig. 3, G and H, and fig. S2) (*13*, *30*). Similar results were seen in staged imaginal discs and when *UAS-tkv*$^{+}$ expression was limited to the wing and the haltere (fig. S2). Conversely, reducing Tkv amounts by uniformly expressing *UAS-tkvRNAi* in wings and halteres increased haltere size by 30 to 60% (Fig. 3, I and J). In a complementary experiment, we reduced *tkv* transcription in the haltere by expressing a known *tkv* repressor, *master of thickveins* (*mtv*) (*32*). In this experiment, we measured haltere discs instead of the adult appendage and found, consistently, that the appendage-generating region of these discs increased in size by ~40% (fig. S2). Thus, different amounts of Tkv not only affect Dpp pathway activation but also affect organ size. The fact that manipulating only Tkv production does not fully transform the sizes of these appendages suggests that additional mechanisms, such as the reduced amounts of *dpp* transcription and the modulation of other morphogen pathways by *Ubx*, also contribute to size regulation. Consistently, when Dpp production is decreased in wing discs that uniformly express *UAS-tkv*$^{+}$, wing size was reduced more than it was by either single manipulation (fig. S3).

***Ubx* regulation of *tkv*.** We next address how *Ubx* up-regulates *tkv* in the haltere. *tkv-lacZ* expression and amounts of Tkv protein were cell-autonomously reduced in medial *Ubx*$^{-}$ clones, whereas lateral *Ubx* mutant tissue retained high amounts of Tkv (Fig. 4, A to D, and fig. S4). Because *tkv* is repressed by Dpp and Hh signaling in the wing (*26*, *30*), these results suggest that, in the haltere, these signals are not able to repress *tkv*. Consistently, activation of the Dpp pathway by expressing a constitutively active form of Tkv (Tkv^{QD}) resulted in cell-autonomous *tkv-lacZ* repression in the wing pouch (Fig. 4, E and F), whereas repression is not observed in the corresponding region of the haltere disc (Fig. 4, G and H).

In *Ubx* mosaic haltere discs, we also found that medial *Ubx*$^{+}$ tissue showed stronger P-Mad staining than *Ubx*$^{-}$ tissue at the same distance from the Dpp source (Fig. 4, A to D). We interpret this observation as evidence that *Ubx*$^{+}$ tissue is more effective at trapping and transducing Dpp than *Ubx*$^{-}$ tissue because of higher Tkv production in *Ubx*$^{+}$ cells.

To further understand the control of *tkv* by *Ubx*, we examined the known *tkv* repressor, *mtv* (*32*). In medial wing disc cells, *mtv* expression is approximately complementary to *tkv* expression (Fig. 4, I and J, and fig. S1), and *mtv*$^{-}$ clones in this region of the wing disc cell autonomously derepressed *tkv* (fig. S4) (*32*). In the haltere, very low *mtv-lacZ* expression was detected in the cells that stained strongly for P-Mad, suggesting that *mtv* is repressed by Dpp in this appendage (Fig. 4, I and J). Accordingly, strong repression of *mtv-lacZ* was seen in *UAS-tkv*^{QD}-expressing haltere pouch clones, whereas weak or no repression was seen in analogous wing clones (Fig. 4, K and L). We also found that, as expected, *Ubx*$^{-}$ clones in the medial haltere cell autonomously derepressed *mtv-lacZ* (fig. S4).

In the wing, Dpp and *mtv* are mandatory repressors of *tkv*: In the absence of either, *tkv* expression is high. In the haltere in the presence of *Ubx*, Dpp is a repressor of *mtv*. Consequently, high levels of these obligate *tkv* repressors (Dpp signaling and *mtv*) do not coexist in the haltere, resulting in *tkv* derepression. Consistent with this model, when we forced *mtv* expression in the medial haltere, where it coexists with Dpp signaling, it repressed *tkv-lacZ* (fig. S4). We note, however, that *Ubx* is likely to control *tkv* through additional means, because *mtv* mutant wing clones did not derepress *tkv-lacZ* expression to

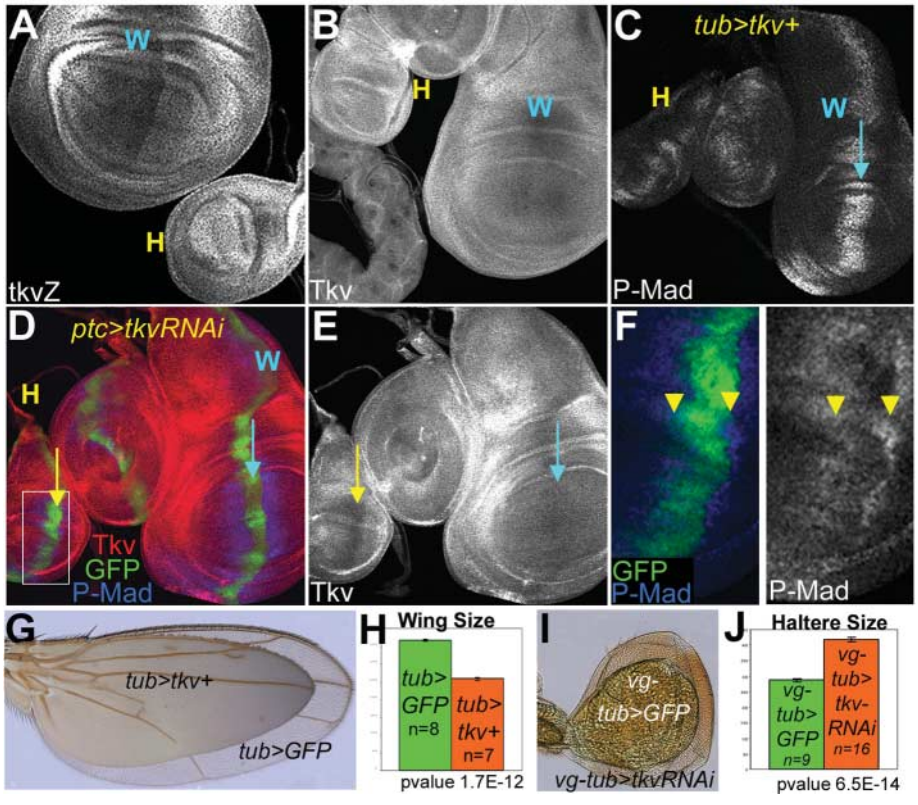

Fig. 3. Tkv production influences Dpp signaling and appendage size. (**A**) *tkv-lacZ* expression was high throughout the haltere, whereas in the wing it was low medially and high laterally. (**B**) Tkv antibody staining showed a pattern similar to that of the *tkv-lacZ* enhancer trap, with less resolution. (**C**) Driving uniform *UAS-tkv*$^{+}$ expression in the wing using *tubGal4* compacted the Dpp activity gradient and created haltere-like P-Mad staining pattern (arrow). (**D** to **F**) Expressing *UAS-tkvRNAi* in the haltere using *ptc-Gal4* (visualized with *UAS-GFP*) reduced Tkv staining [yellow arrow in (D) and (E)] and resulted in a bimodal P-Mad staining pattern [yellow arrowheads in (F), which shows a magnification of the region boxed in (D)]. (**G**) Adult wings uniformly expressing *UAS-tkv*$^{+}$ using *tubGal4* were ~30% smaller than control wings. (**H**) Quantification of wing size reduction caused by uniform *UAS-tkv*$^{+}$ expression (orange) compared to controls (green). Error bars indicate SEM. (**I**) Adult halteres uniformly expressing *UAS-tkvRNAi* using *vg-tubGal4* were up to 60% larger than control halteres. (**J**) Quantification of haltere size increase caused by uniform *tkvRNAi* expression (orange) compared to controls (green). The average increase seen is 46%.

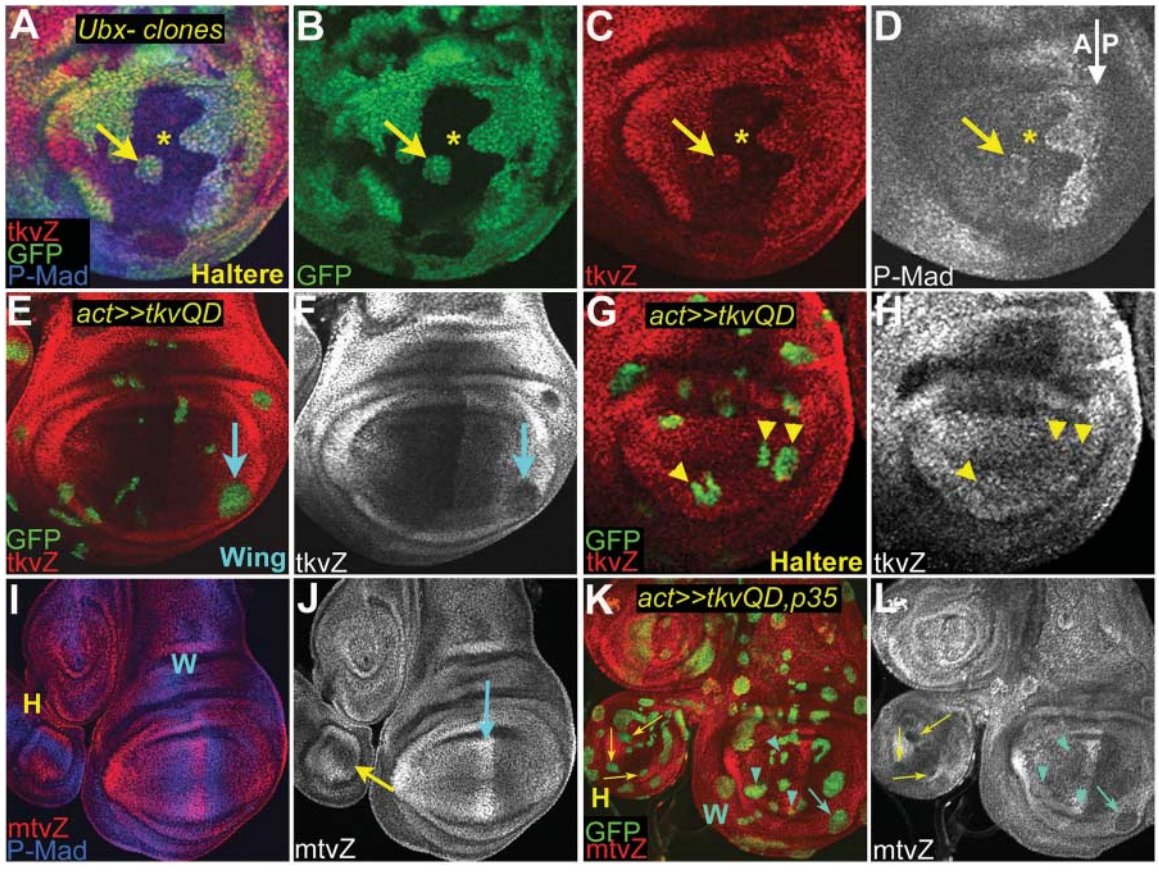

Fig. 4. Dpp and *Ubx* collaborate to repress a *tkv* repressor in the haltere. (**A** to **D**) *Ubx* mutant tissue in the medial haltere (absence of GFP) shows a cell-autonomous reduction in *tkv-lacZ* and reduced P-Mad staining. High P-Mad and *tkv-lacZ* staining can be detected in a Ubx^{+} island (yellow arrow) that is separated from Dpp-producing cells by Ubx^{-} tissue (*). The approximate position of the AP boundary is indicated by a white arrow in (D). (**E** to **H**) Clones expressing *UAS-tkv*^{QD} (marked with GFP) repress *tkv-lacZ* in the wing pouch (cyan arrow) but not in the analogous domain of the haltere (yellow arrowheads). (**I** and **J**) Wild-type wing and haltere discs stained for *mtv-lacZ* and P-Mad. *mtv-lacZ* is strongly expressed in Dpp-producing cells of the wing (cyan arrow) but is repressed in Dpp-producing cells of the haltere (yellow arrow). (**K** and **L**) Clones expressing *UAS-tkv*^{QD} (marked with GFP) strongly repress *mtv-lacZ* in the haltere (yellow arrows). Similar clones in the wing repress *mtv-lacZ* moderately in the P compartment (cyan arrow) and not at all in the A compartment (cyan arrowheads).

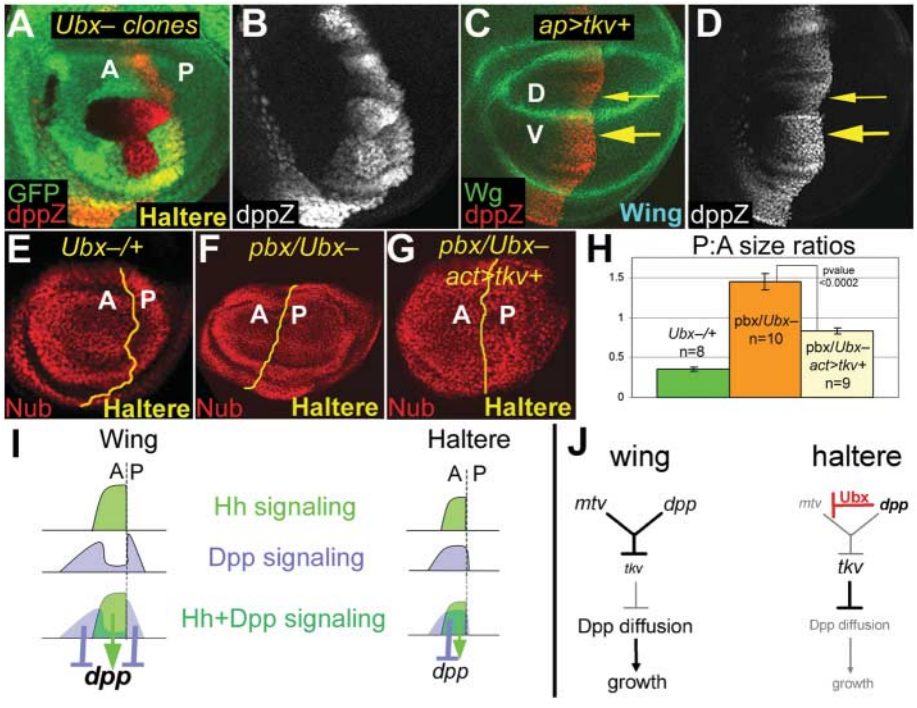

Fig. 5. Contributions of *dpp* transcription and mobility to growth. (**A** and **B**) *dpp-lacZ* is up-regulated in *Ubx* mutant haltere tissue (marked by loss of GFP) within the AP organizer. (**C** and **D**) *UAS-tkv*$^{+}$ expression in dorsal cells using *ap-Gal4* results in *dpp-lacZ* down-regulation (thin arrow) compared with ventral cells (thick arrow). (**E** to **G**) Examples of $+/Ubx^{-}$ (E), pbx/Ubx^{-} (F), and pbx/Ubx^{-}; *actGal4>tkv*$^{+}$ (G) haltere discs stained for Nubbin (Nub), a marker of the appendage, and a marker of the AP compartment boundary (yellow line). (**H**) P:A ratios of the Nub domains of $+/Ubx^{-}$, pbx/Ubx^{-}, and pbx/Ubx^{-}; *actGal4>tkv*$^{+}$ haltere discs. Error bars indicate SEM. (**I**) Summary of the consequences of different spatial relationships of Dpp and Hh signaling for *dpp* transcription in the wing and haltere. (**J**) Summary of how Dpp represses *mtv* in the presence of *Ubx* to control *tkv* expression, Dpp mobility, and growth in the haltere compared with the wing.

haltere levels (fig. S4), and ectopic *mtv* in the haltere did not repress *tkv-lacZ* expression to the extent seen in the medial wing (fig. S4).

Control of the relative position of Dpp and Hh signaling by *tkv* regulation. Because of high Tkv production in the wild-type haltere disc, peak Dpp signal transduction occurs in the AP organizer, the same cells that transduce the Hh signal. Thus, in the haltere, the activity

profiles for these two signal transduction pathways coincide with each other (Fig. 1, F to H, and 5I). In contrast, low *tkv* expression in the wing AP organizer results in two peaks of Dpp signaling that are on either side of Hh-transducing cells. This difference will have important consequences for the expression of genes that are targets of both pathways. For example, *dpp* is activated by Hh and repressed by Dpp signaling (*19*–*22*, *33*). In the haltere, these two conflicting inputs occur in the same cells, possibly contributing to reduced *dpp* expression compared with the wing. Ubx^- clones cell-autonomously up-regulated *dpp-lacZ* in the haltere (Fig. 5, A and B). To test whether *Ubx* lowers *dpp* transcription in part by aligning Dpp and Hh signaling, we expressed uniform *UAS-*tkv^+ in the dorsal half of the wing disc. As a result, in this region of the wing disc both signals peaked in the same cells, and *dpp-lacZ* expression was reduced compared with the ventral half of these wing discs (Fig. 5, C and D, and fig. S5). Conversely, expressing *tkvRNAi* in dorsal haltere cells increased *dpp-lacZ* expression (fig. S5). Thus, *Ubx* reduces *dpp* transcription in part by changing where peak Dpp signaling occurs in the disc (Fig. 5I). We note that *Ubx* is likely to reduce *dpp* expression in additional ways, because increasing *tkv* expression does not lower *dpp-lacZ* expression to that observed in wild-type haltere. Nevertheless, varying the relative spatial relationships between signal transduction pathways is a potentially powerful mechanism for modifying the outputs from commonly used pathways. We suggest that selector genes may work through molecules that control ligand distribution to vary the spatial relationships between these and other signal transduction pathways in diverse contexts during development.

Dpp mobility versus *dpp* transcription. The finding that increased *tkv* expression results in decreased *dpp* transcription reveals an unexpected link between Dpp mobility and Dpp production. Because of this link, the above experiments do not discriminate between growth effects due to differences in Dpp mobility per se as opposed to secondary consequences on Dpp production. To distinguish between these scenarios, we made use of a compartment-specific *Ubx* regulatory allele, *posterior bithorax* (*pbx*), that lacks detectable Ubx in the P compartment when paired with a *Ubx* null allele but still has normal *Ubx* expression in the A compartment (fig. S6) (*8*). Consequently, in *pbx*/Ubx^- haltere discs, the P compartment increased in size such that the P:A size ratio was 1.45 (Fig. 5, E and F); the P:A ratio of +/Ubx^- haltere discs was ~0.35 (*13*). We suggest that Dpp more readily diffuses into and through the P compartments of *pbx*/Ubx^- discs because of the wing-like expression pattern of *tkv* and that this wing-like diffusion results in its robust growth.

To test whether differences in Tkv-regulated Dpp diffusion affect tissue growth independently of an effect on Dpp production, we examined the consequences of expressing *UAS-*tkv^+ uniformly in *pbx*/Ubx^- haltere discs. If Tkv's effect on growth is mediated only by lowering Dpp production, both compartments should be reduced in size and thus maintain the same size ratio. However, if reducing Dpp mobility directly affects growth, the P compartment should be reduced in size more than the A compartment, which, in *pbx*/Ubx^- discs, already has high *tkv* expression. We found that expressing uniform tkv^+ in *pbx*/Ubx^- discs decreased the size of the P compartment more than the A compartment, resulting in a P:A ratio of 0.83 (Fig. 5, E to H). Because uniform tkv^+ returned the P:A ratio back to the wild-type ratio by ~56% (from 1.45 to 0.83, whereas +/Ubx^- discs have a P:A ratio of ~0.35), these results suggest that this single variable is sufficient to provide ~50% rescue of the size of an otherwise *Ubx* mutant P compartment.

Discussion. We have investigated the mechanism underlying a classic yet poorly understood phenomenon in biology: how size variations are genetically programmed in animal development. Many experiments show that organ size is not governed by counting cell divisions but instead depends on disc-intrinsic yet cell-nonautonomous mechanisms, possibly relying on morphogen signaling (*34*). Our results support this idea by showing that alterations in a morphogen gradient contribute to size differences between appendages. In the example investigated here, *Ubx* limits the size of the haltere by reducing both Dpp production and Dpp mobility. Moreover, both of these effects are due, in part, to higher *tkv* expression in the medial haltere (Fig. 5, I and J). In many morphogen systems, the receptors themselves have been shown to control the distribution of the ligand and, consequently, pathway activation (*30*, *35*–*37*). We show that a selector gene exploits this phenomenon to modify organ size.

Although the mechanism by which Dpp controls proliferation is not fully understood, recent results argue that, in the medial wing disc, cells may compare the amount of Dpp transduction with their neighbors, whereas lateral cells proliferate in response to absolute Dpp levels (*17*). Our results suggest several ways in which the altered Dpp gradient in the haltere could limit its growth. First, proliferation of lateral haltere cells may be limited because they perceive less Dpp. Second, the narrower Dpp gradient results in fewer cells exposed to the gradient in the medial haltere. Another notable difference is that, because there are two peaks of Dpp signaling in the wing but only one in the haltere, the wing has four distinct slopes whereas the haltere has only two. The less complex Dpp activity landscape of the haltere may also contribute to its reduced growth.

On the basis of these results, we suggest that altering the shape and intensity of morphogen gradients may be a general mechanism by which selector genes affect tissue sizes in animal development. Consistent with this view, *wingless* (*wg*), another long-range morphogen in the wing, is partially repressed in the haltere (*38*). Intriguingly, some of the size and shape differences in the beaks of Darwin's finches are controlled by alterations in the production of the Dpp ortholog BMP4 (*39*). Our results suggest that differences in the diffusion of this ligand may also contribute to the range of beak morphologies that have evolved in these species.

References and Notes

1. P. R. Grant, B. R. Grant, *Curr. Biol.* **15**, R614 (2005).
2. J. Zakany, D. Duboule, *Cell Tissue Res.* **296**, 19 (1999).
3. D. M. Wellik, M. R. Capecchi, *Science* **301**, 363 (2003).
4. R. Krumlauf, *Cell* **78**, 191 (1994).
5. A. C. Burke, C. E. Nelson, B. A. Morgan, C. Tabin, *Development* **121**, 333 (1995).
6. M. Kessel, P. Gruss, *Cell* **67**, 89 (1991).
7. S. B. Carroll, S. D. Weatherbee, J. A. Langeland, *Nature* **375**, 58 (1995).
8. E. B. Lewis, *Nature* **276**, 565 (1978).
9. P. A. Beachy, S. L. Helfand, D. S. Hogness, *Nature* **313**, 545 (1985).
10. S. M. Cohen, in *The Development of* Drosophila melanogaster, M. Bate, A. Martinez Arias, Eds. (Cold Spring Harbor Laboratory Press, Cold Spring Harbor, NY, 1993), vol. II, pp. 747–842.
11. P. Martin, *J. Exp. Zool.* **222**, 97 (1982).
12. F. Roch, M. Akam, *Development* **127**, 97 (2000).
13. See Materials and Methods on *Science* Online.
14. G. Morata, A. Garcia-Bellido, W. Roux, *Arch. Dev. Biol.* **179**, 125 (1976).
15. T. Lecuit *et al.*, *Nature* **381**, 387 (1996).
16. D. Nellen, R. Burke, G. Struhl, K. Basler, *Cell* **85**, 357 (1996).
17. D. Rogulja, K. D. Irvine, *Cell* **123**, 449 (2005).
18. P. A. Lawrence, G. Struhl, *Cell* **85**, 951 (1996).
19. K. Basler, G. Struhl, *Nature* **368**, 208 (1994).
20. I. Guillen *et al.*, *Development* **121**, 3447 (1995).
21. T. Tabata, C. Schwartz, E. Gustavson, Z. Ali, T. B. Kornberg, *Development* **121**, 3359 (1995).
22. M. Zecca, K. Basler, G. Struhl, *Development* **121**, 2265 (1995).
23. R. Burke, K. Basler, *Development* **122**, 2261 (1996).
24. J. Capdevila, I. Guerrero, *EMBO J.* **13**, 4459 (1994).
25. J. J. Sekelsky, S. J. Newfeld, L. A. Raftery, E. H. Chartoff, W. M. Gelbart, *Genetics* **139**, 1347 (1995).
26. H. Tanimoto, S. Itoh, P. ten Dijke, T. Tabata, *Mol. Cell* **5**, 59 (2000).
27. E. V. Entchev, A. Schwabedissen, M. Gonzalez-Gaitan, *Cell* **103**, 981 (2000).
28. A. A. Teleman, S. M. Cohen, *Cell* **103**, 971 (2000).
29. T. Y. Belenkaya *et al.*, *Cell* **119**, 231 (2004).
30. T. Lecuit, S. M. Cohen, *Development* **125**, 4901 (1998).
31. T. J. Brummel *et al.*, *Cell* **78**, 251 (1994).
32. Y. Funakoshi, M. Minami, T. Tabata, *Development* **128**, 67 (2001).
33. T. E. Haerry, O. Khalsa, M. B. O'Connor, K. A. Wharton, *Development* **125**, 3977 (1998).
34. S. J. Day, P. A. Lawrence, *Development* **127**, 2977 (2000).
35. K. M. Cadigan, M. P. Fish, E. J. Rulifson, R. Nusse, *Cell* **93**, 767 (1998).
36. J. Casanova, G. Struhl, *Nature* **362**, 152 (1993).
37. Y. Chen, G. Struhl, *Cell* **87**, 553 (1996).
38. S. D. Weatherbee, G. Halder, J. Kim, A. Hudson, S. Carroll, *Genes Dev.* **12**, 1474 (1998).

39. A. Abzhanov, M. Protas, B. R. Grant, P. R. Grant, C. J. Tabin, *Science* **305**, 1462 (2004).
40. Y. S. Lee, R. W. Carthew, *Methods* **30**, 322 (2003).
41. We thank S. Cohen, M. Gonzalez-Gaitan, T. Jessell, L. Johnston, E. Laufer, B. McCabe, M. O'Connor, G. Struhl, T. Tabata, the Bloomington Stock Center, and the Developmental Studies Hybridoma Bank for antibodies and fly stocks and R. Axel, O. Hobert, T. Jessell, L. Johnston, D. Rogulja, and G. Struhl for comments on the manuscript. This work was supported by a grant from the NIH to R.S.M. and an NIH training grant (M.A.C.).

Supporting Online Material
www.sciencemag.org/cgi/content/full/1128650/DC1
Materials and Methods
SOM Text
Figs. S1 to S6

12 April 2006; accepted 25 May 2006
Published online 1 June 2006;
10.1126/science.1128650
Include this information when citing this paper.

Hierarchical Action and Inhibition of Plant Dicer-Like Proteins in Antiviral Defense

Angélique Deleris,[1] Javier Gallego-Bartolome,[1] Jinsong Bao,[2] Kristin D. Kasschau,[2] James C. Carrington,[2] Olivier Voinnet[1]*

The mechanisms underlying induction and suppression of RNA silencing in the ongoing plant-virus arms race are poorly understood. We show here that virus-derived small RNAs produced by *Arabidopsis* Dicer-like 4 (DCL4) program an effector complex conferring antiviral immunity. Inhibition of DCL4 by a viral-encoded suppressor revealed the subordinate antiviral activity of DCL2. Accordingly, inactivating both DCL2 and DCL4 was necessary and sufficient to restore systemic infection of a suppressor-deficient virus. The effects of DCL2 were overcome by increasing viral dosage in inoculated leaves, but this could not surmount additional, non–cell autonomous effects of DCL4 specifically preventing viral unloading from the vasculature. These findings define a molecular framework for studying antiviral silencing and defense in plants.

In RNA silencing, ribonuclease (RNase) III–like enzymes in the Dicer family produce short interfering (si)RNA and micro (mi)RNA from RNA with double-stranded (ds) features (*1*). These molecules guide RNA-induced silencing complexes (RISCs) to suppress gene expression at the transcriptional, RNA-stability, and translational levels (*2*). *Arabidopsis thaliana* has four specialized Dicer-like (DCL) proteins. DCL1 processes fold-back precursors to release miRNAs (*3*). DCL3 produces 24–nucleotide (nt)–long, DNA repeat–associated siRNAs guiding heterochromatin formation (*4*). DCL4 generates 21-nt-long siRNAs that mediate posttranscriptional silencing of some endogenous genes [trans-acting (ta)–siRNAs; (*5*, *6*)] and of transgenes mediating RNA interference (*7*). DCL2 synthesizes stress-related natural-antisense-transcript (nat)–siRNAs (*8*), siRNAs derived from at least one virus (*4*), and, in *dcl4* mutant plants, it alternately processed ~22-nt siRNAs from ta-siRNA precursors (*5*, *6*).

The observations that virus-derived siRNAs accumulate in plant and insect infected tissues and that many viruses encode suppressor proteins targeting DCL, RISC, or small RNA activities strongly suggest that RNA silencing has antiviral roles (*9*–*11*). In plants, one or more of the six RNA-dependent RNA-polymerase (RDR) paralogs, including *Arabidopsis* RDR6 and RDR1, may strengthen primary silencing responses by producing dsRNA from viral templates (*12*) and by amplifying mobile silencing signals conditioning antiviral immunity in non-infected tissues (*7*, *13*). Nevertheless, the genetic bases of silencing induction and suppression by plant viruses remain unclear. Even the existence of an antiviral RISC ("slicer") is arguable because DCL-mediated processing of virus-derived dsRNA could be, in principle, sufficient to dampen infections. It remains also uncertain how, when, and where antiviral silencing and its suppression impact susceptibility and defense in whole plants. This study addresses these issues using *Arabidopsis* silencing mutants and three distinct RNA viruses.

DCL4- and DCL2-dependent siRNAs recruit an antiviral RISC. *Arabidopsis* plants were inoculated with modified *Tobacco rattle virus* (TRV-PDS) (Fig. 1A) containing a fragment of the *Arabidopsis* phytoene desaturase (*PDS*) gene in place of the RNA2-encoded 2b and 2c sequences. Like TRV-infected tissues (Fig. 1B), TRV-PDS–infected tissues are free of disease symptoms, because of a strong silencing response that dramatically reduces viral titers (*14*), and exhibit extensive photobleaching due to virus-induced gene silencing (VIGS) of *PDS* (Fig. 1C) (*7*).

TRV-PDS–specific siRNAs accumulated as discrete 21-nt and 24-nt species in wild-type (WT) *Arabidopsis* (Fig. 1D), a pattern unchanged in *rdr1*, *rdr2*, *rdr6* [supporting online material (SOM), fig. S1], and *dcl2* mutants (Fig. 1D). However, the 24-nt and 21-nt siRNAs were undetectable in *dcl3* and *dcl4* mutants, respectively. Loss of 21-nt siRNAs coincided with appearance of 22-nt siRNAs in *dcl4* mutants (Fig. 1D). Identical siRNA patterns were detected with an RNA2(TRV)-specific probe, whereas probes specific for cellular *PDS* sequences absent in TRV-PDS

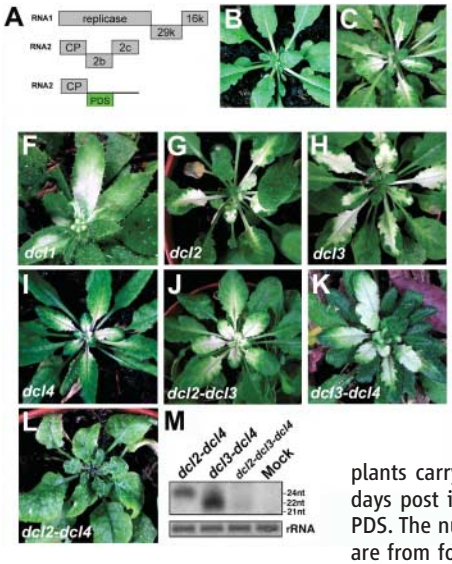

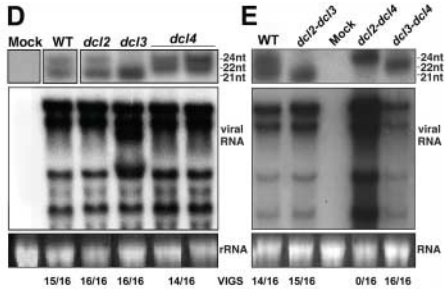

Fig. 1. (**A**) Genome organization of TRV and its TRV-PDS derivative. (**B** and **C**) Asymptomatic infection (B) and extensive photobleaching (C) caused by TRV and TRV-PDS, respectively. (**D** and **E**) Analysis of (top) low- and (bottom) high-molecular-weight RNAs from TRV-PDS–infected plants carrying single (D) and double (E) *dcl* mutations [14 days post inoculation (dpi)]. The probe was specific for viral PDS. The numbers of infected plants showing photobleaching are from four independent experiments involving four plants each. (**F** to **L**) Disease symptoms and VIGS in *dcl* mutants (14 dpi). (**M**) TRV-PDS siRNA analysis in *dcl2-dcl3-dcl4* triple mutants (14 dpi). rRNA shown by ethidium bromide staining.

[1]Institut de Biologie Moléculaire des Plantes, CNRS Unité Propre de Recherche (UPR) 2357, 12, rue du Général Zimmer, 67084 Strasbourg Cedex, France. [2]Center for Genome Research and Biocomputing, Oregon State University, Corvallis, OR 97331, USA.

*To whom correspondence should be addressed. E-mail: olivier.voinnet@ibmp-ulp.u-strasbg.fr

www.sciencemag.org/cgi/content/full/1128650/DC1

Supporting Online Material for

Hox Control of Organ Size by Regulation of Morphogen Production and Mobility

Michael A. Crickmore, Richard S. Mann*

*To whom correspondence should be addressed. E-mail: rsm10@columbia.edu

Published 1 June 2006 on *Science* Express
DOI: 10.1126/science.1128650

This PDF file includes:

Supplementary Online Information:

Materials and Methods

Fly Strains

Ubx mutant clones: *Ubx*$^{9\text{-}22}$ was recombined with *FRT82B* and crossed *to hsflp; FRT82B Ub-GFP flies*. To generate a high frequency of clones (e.g. Fig. 3A), we used *vg-Gal4 UAS-flp* to induce recombination. The clones in Fig. 1D grew for 72 hours after induction whereas the clones we scored for size ratios (Fig. 1E) grew for 48 hours. To generate haltere discs with more than 50% *Ubx* mutant tissue, we used heat shock-induced flp and the Minute technique to induce clones 48-72 hours into development.

UAS-tkvRNAi was generated by cloning the final exon of *tkv* as and inverted repeat into the pWIZ vector (*41*). To increase potency, all crosses involving *UAS-tkvRNAi* were grown at 30°C or with two copies of *UAS-tkvRNAi*.

TkvQD clones were generated by heat-shocking hsflp; act>CD2>Gal4, UAS-GFP/UAS-tkvQD flies at 48-72 hours of development. Dpp::GFP expressing clones were generated in a similar manner except an act>y>Gal4 transgene was used and the flies were transferred to 18ºC after clone induction to limit Dpp::GFP production.

To express *dpp* in the AP organizers of the wing and haltere while avoiding embryonic lethality, *ptc-Gal4 UAS-GFP; G80*^{ts} flies were crossed to *UAS-dpp*. The cross was raised at 18ºC for two days and then shifted to 30ºC for three days prior to dissection.

To avoid the lethality associated with uniform *tkv-RNAi* expression, we created a driver that is active in most haltere and wing cells during larval stages. The *vg-tub-Gal4* driver consists of *vg-Gal4*, *UAS-flp*, *tub>CD2>Gal4*, and *UAS-GFP* all recombined onto the

second chromosome. See Fig. S2G and H for expression in the haltere, similar expression is seen in the wing.

Uniform *tkv+* levels were driven throughout the fly by crossing *UAS-tkv+* flies to *act-Gal4* or *tub-Gal4*.

To reduce cell death, UAS-tkv^{QD} clones were generated in combination with *UAS-p35* as indicated.

***dpp tkv* and *mtv* reporters:**

dpp-lacZ^{10638}*/Cyo-GFP*

tkv-lacZ/Cyo-GFP (27)

mtv-lacZ/Cyo-GFP

Gal4 lines:

tub-Gal4/TM6B

ap-Gal4 dpp-lacZ^{10638}

act>CD2>Gal4 UAS-GFP (III)

hsflp; UAS-GFP; act>y>Gal4

***Ubx, dpp,* and *mtv* alleles:**

pbx/TM6B

act-Gal4 UAS-GFP; pbx/TM6B

TM2 (Ubx–)/TM6B

FRT42D mtv^{6}

dpp^{his4}/CyoGFP; UAS-tkv

dpp^{d6}/CyoGFP; tub-Gal4/TM6B

Others:

hsflp; UAS-tkv^{QD} (III)

hsflp; UAS-p35; UAS-tkv^{QD}

UAS-tkv+; TM2/TM6B

UAS-dpp::GFP (III)

Antibody Staining

We used standard procedures with the exception of the extracellular GFP staining for which the protocol of (*30*) was used.

Antibodies used: Rabbit anti-GFP 1:1000 (Molecular Probes), Rabbit anti-βGal 1:10,000 (Cappel), Rat anti-Moira 1:5000 (B. Noro), Rabbit anti-P-Mad 1:1000 (E. Laufer and T. Jessell), Guinea Pig anti-P-Mad 1:1250 (E. Laufer and T. Jessell), Mouse anti-Nub 1:10 (S. Cohen), Mouse anti-Ubx 1:20, Rabbit anti-Tkv (B. McCabe and M. O'Connor)

Size Measurements

All sizes were measured as pixel counts using Adobe Photoshop. For adult wings and halteres only the blade or capitellum of females was measured. For *tkv* and *tkvRNAi* overexpression, animals were raised under non-crowding conditions. Eggs were collected for two hours and grown for ~48 hours. 50 first instar larvae were transferred to fresh tubes and

grown until dissection or eclosure. Larvae expressing UAS-tkv+ were developmentally staged to their controls by dissecting wandering larvae when 18 to 25 of the 50 larvae were wandering. Mtv overexpressing larvae and their controls were dissected at 98-100 hours of development. The size of the Nubbin domain was measured as the haltere or wing primordium size in imaginal discs. Flies mutant for *dpp* while overexpressing *tkv+* rarely eclose, so eggs from this cross were collected for 24 hours and grown without transfering larvae. Measurements of *Ubx–* vs. twin spot clone sizes and P:A ratios were internally controlled and performed on animals grown under normal conditions for 96-120 hours. Nubbin domain sizes were measured blind, without knowledge of the genotype. Error bars are Standard Error of the Mean.

Supplementary Notes

1. Both BrdU labeling experiments and mitotic clonal analysis show that cells in both the haltere and wing discs continue to divide throughout larval development, including the mid to late 3rd instar stage.
2. The magnitude of increased growth seen in discs with *Ubx– M+* tissue (e.g. Figure 1C) depends on the percentage of tissue mutant and, likely, the position of the mutant tissue in the disc.
3. The wing and haltere expression patterns described in the late third instar for *mtv-lacZ*, *dpp-lacZ*, *tkv-lacZ*, and P-Mad are also observed in early third instar discs, but are scaled according to disc size.

Supplementary Figure Legends:

Supplementary Figure 1. Quantifying Dpp Pathway Gene Expression in the Haltere and Wing.

(A-E) Shown are traces of the relative expression levels of P-Mad, *dpp-lacZ*, *tkv-lacZ* Tkv protein, and *mtv-lacZ* along the AP axes of wild type haltere (red) and wing (blue) late third instar discs. For all graphs, the X axis (from left to right) begins at the anterior edge of the pouch and ends at the posterior edge of the pouch; the approximate position of the AP boundary is indicated (arrows). The Y axis shows the relative pixel intensity. For each readout, the haltere and wing traces were taken from the same image (shown on the left) and are therefore directly comparable. Images were imported into ImageJ and pixels were measured by boxing a subset of the pouch regions of the discs.

(F and G) Blown up images focused on the wing and haltere pouch regions stained for *mtv-lacZ.*

(H) A cartoon describing some relevant domains in the wing imaginal disc.

Supplementary Figure 2. Tkv Levels Do Not Affect Cell Size.

(A and B) Shown are high magnification pictures of *tub-Gal4 UAS-GFP* and *tub-Gal4 UAS-tkv+* adult wings in the region posterior to vein L5. As each wing cell produces a single hair, counting the number of hairs in a given area provides a measure of cell number in that area and, therefore, cell size.

(C) Cell size is the same when *tkv+* is overexpressed in wings as it is in control wings.

(D) A control wing expressing *UAS-GFP* with *vg-tub-Gal4*.

(E) Driving *UAS-tkv+* in only the wing and haltere reduces wing size.

(F) In contrast to an increase in haltere size, wing size is reduced when *UAS-tkvRNAi* is expressed with *vg-tub-Gal4*, perhaps due to a reduction in already limiting amounts of this receptor.

(G-I) Wing discs expressing *GFP* or *tkv+* with *tub-Gal4* and stained for Nubbin (Nub), which labels the cells fated to form the appendage, and P-Mad to demonstrate Dpp pathway activation. The Nub domain in wings over-expressing *tkv+* is ~40% smaller than controls (I).

(J-L) Here the *tkv* repressor, *mtv*, is used to reduce levels of *tkv* in the haltere disc. Haltere discs in which *GFP* (J) or *mtv* and *GFP* (K) are driven by *vg-tub-Gal4* stained for Nubbin and GFP. *vg-tub-Gal4* drives expression of Gal4 in most cells of the wing and haltere discs with small, random patches of cells lacking expression (non-green). The Nub domain is 40% larger in haltere discs over-expressing *mtv* (L). Overgrowth due to expression of *tkv-RNAi* in the haltere leads to excessive folding of the Nub domain, making quantification of disc sizes difficult.

Supplementary Figure 3. Decreasing Dpp production and mobility.

(A) Control wing.

(B) As also shown in Fig. 3E, wing size is reduced with *tkv+* overexpression.

(C) Dpp production is reduced in the trans-allelic combination dpp^{his4}/dpp^{d6}, resulting in decreased wing size.

(D) The combination of decreased Dpp and increased Tkv levels results in a greater size reduction than either manipulation alone.

(E) When *tkv* is overexpressed in a *dpp* hypomorphic background, wings decrease 40% in size compared to control wings.

Supplementary Figure 4. Control of *tkv* through *mtv* in the haltere.

(A and B) *Ubx*– clone (arrow) in the medial haltere shows lower levels of Tkv protein than surrounding wild type tissue.

(C-E) *mtv* mutant clones (arrow, lack of GFP) in the medial wing derepress *tkv-lacZ.* P-Mad levels are also higher in the *mtv* clones. *tkv-lacZ* levels in these clones are still lower than those found in the lateral wing, suggesting that other *tkv* repressors exist.

(F and G) Consistent with the wild type expression patterns in the wing and haltere, medial *Ubx*– clones (absence of GFP) derepress *mtv-lacZ* cell autonomously.

(H and I) Clones overexpressing *mtv* (marked by GFP and outlined) in the haltere repress *tkv-lacZ.*

Supplementary Figure 5. Tkv levels affect *dpp* transcription.

(A and B) A control *ap-Gal4* wing disc stained for *dpp-lacZ* and Wg to mark the DV boundary. Here and throughout Dorsal (D; *ap-Gal4* expressing) cells are above the DV Wg stripe are Dorsal (D) *ap-Gal4* expressing cells while Ventral (V; *ap-Gal4* non-expressing) cells, are below the Wg stripe. *dpp-lacZ* is expressed at similar levels on both sides of the DV boundary.

(C and D) As also shown in Fig. 5B, *dpp-lacZ* decreases in dorsal wing disc cells expressing *UAS-tkv+* with *ap-Gal4.*

(E and F) A control *ap-Gal4* expressing haltere disc showing similar *dpp-lacZ* levels in D and V cells.

(G and H) *dpp-lacZ* is increased in dorsal cells when *UAS-tkvRNAi* is driven with ap-Gal4.

(I) Cartoon summarizing the expression pattern of *ap-Gal4* (blue) relative to Wg (green).

Supplementary Figure 6. The *pbx* mutant.

(A) Wing and haltere discs heterozygous for the *Ubx* null mutation on the *TM2* balancer chromosome stained for Ubx and *dpp-lacZ* to mark the AP boundary. The bottom panel shows only the red (*dpp-lacZ*) channel.

(B) Ubx staining is lost in the P compartment of *pbx/Ubx-* discs. The bottom panel shows only the red (*dpp-lacZ*) channel. Note the higher levels of *dpp-lacZ* expression even though the A compartment still expresses *Ubx*.

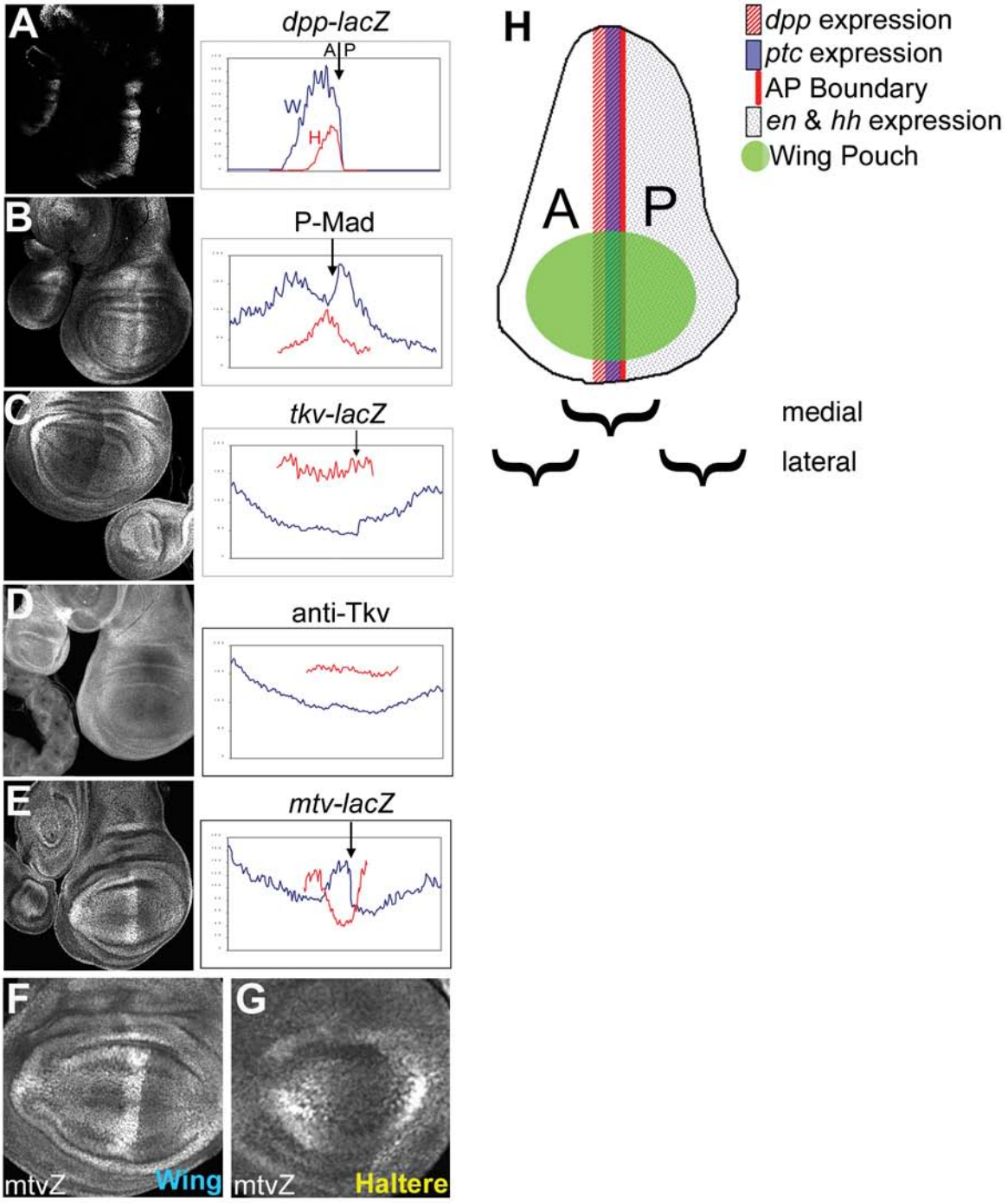
A
dpp-lacZ
A P
W
H
B
P-Mad
C
tkv-lacZ
D
anti-Tkv
E
mtv-lacZ
F
mtvZ
Wing
G
mtvZ
Haltere
H
dpp expression
ptc expression
AP Boundary
en & hh expression
Wing Pouch
A
P
medial
lateral

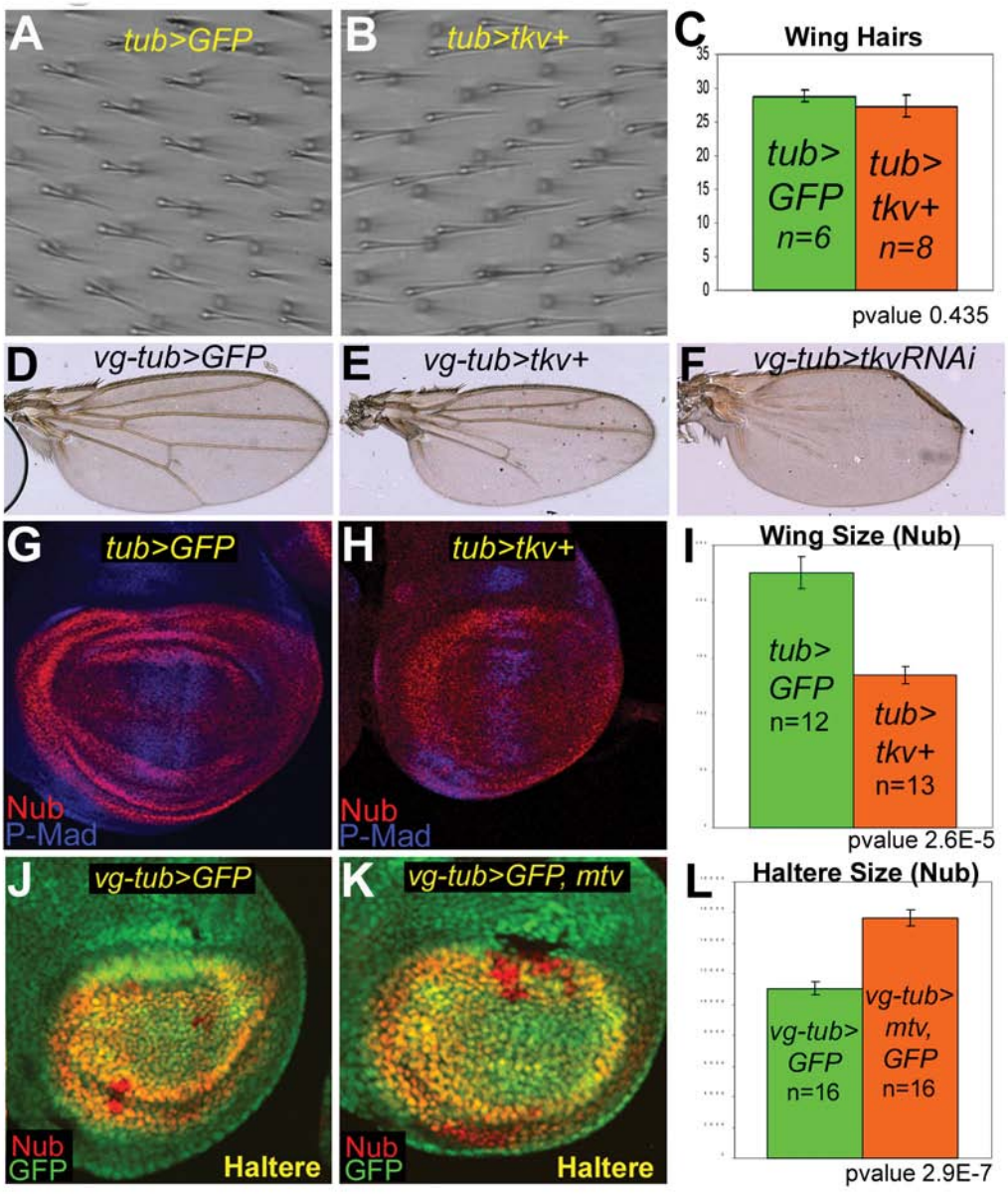
A
tub>GFP
B
tub>tkv+
C
Wing Hairs
35
30
25
20
15
10
5
0
tub>
GFP
n=6
tub>
tkv+
n=8
pvalue 0.435
D
vg-tub>GFP
E
vg-tub>tkv+
F
vg-tub>tkvRNAi
G
tub>GFP
Nub
P-Mad
H
tub>tkv+
Nub
P-Mad
I
Wing Size (Nub)
tub>
GFP
n=12
tub>
tkv+
n=13
pvalue 2.6E-5
J
vg-tub>GFP
Nub
GFP
Haltere
K
vg-tub>GFP, mtv
Nub
GFP
Haltere
L
Haltere Size (Nub)
vg-tub>
GFP
n=16
vg-tub>
mtv,
GFP
n=16
pvalue 2.9E-7

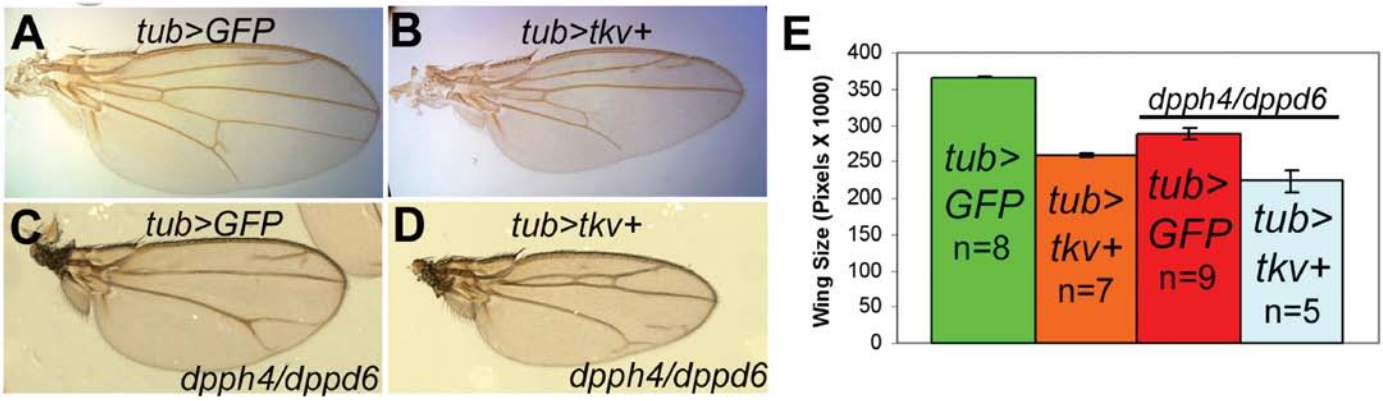
A
tub>GFP
B
tub>tkv+
C
tub>GFP
dpph4/dppd6
D
tub>tkv+
dpph4/dppd6
E
Wing Size (Pixels X 1000)
400
350
300
250
200
150
100
50
0
dpph4/dppd6
tub>
GFP
n=8
tub>
tkv+
n=7
tub>
GFP
n=9
tub>
tkv+
n=5

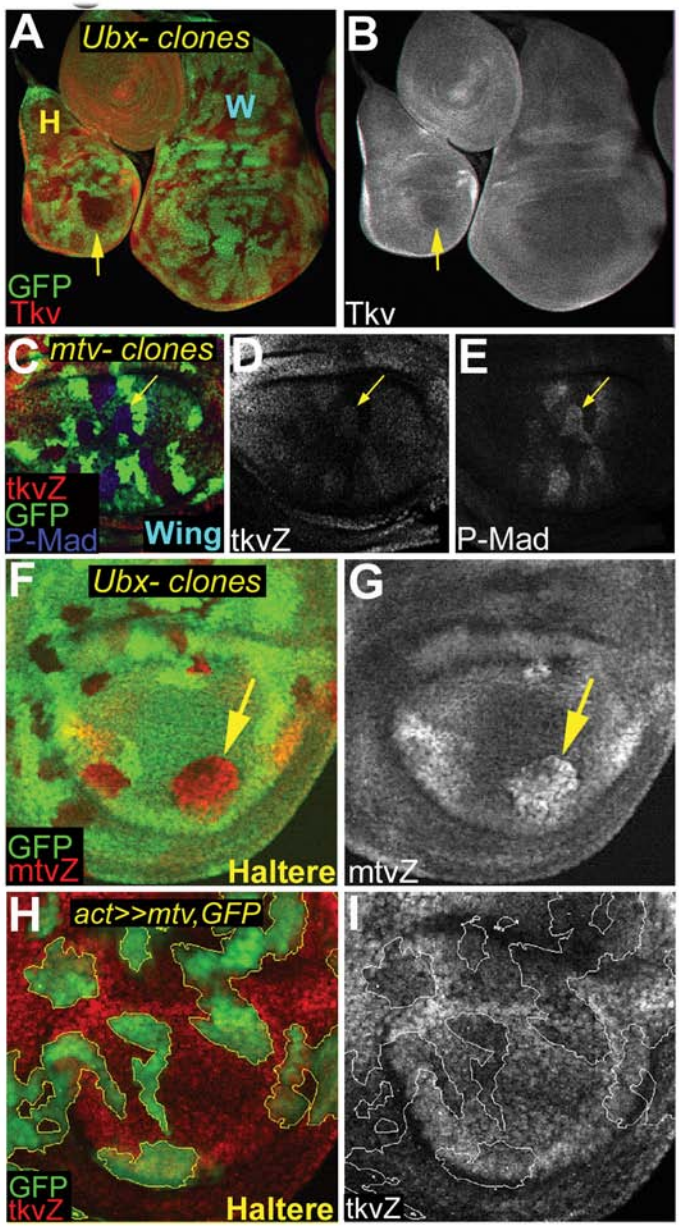
A
Ubx- clones
H
W
GFP
Tkv
B
Tkv
C
mtv- clones
tkvZ
GFP
P-Mad
Wing
D
tkvZ
E
P-Mad
F
Ubx- clones
GFP
mtvZ
Haltere
G
mtvZ
H
act>>mtv,GFP
GFP
tkvZ
Haltere
I
tkvZ

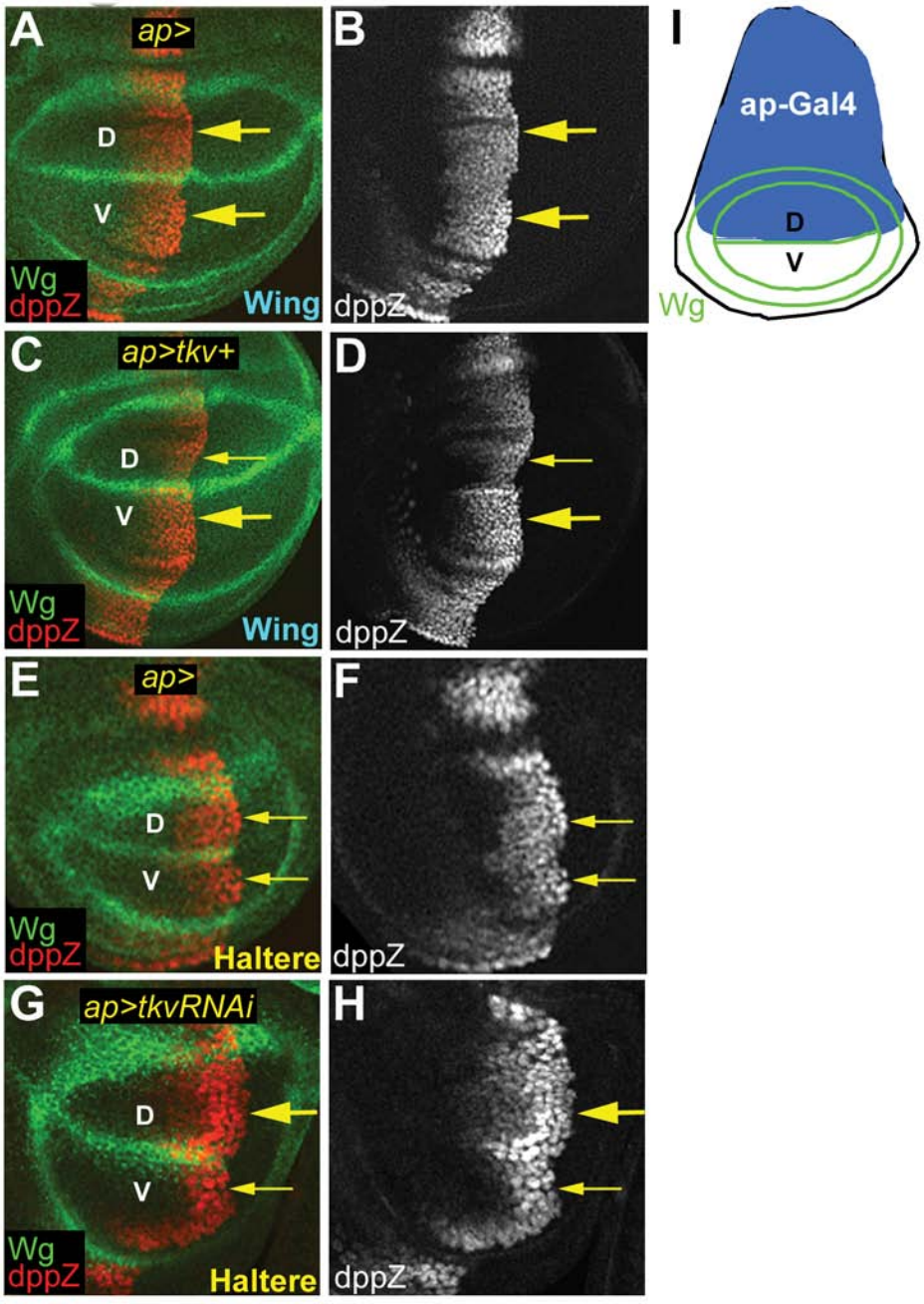
A
ap>
D
V
Wg
dppZ
Wing
B
dppZ
I
ap-Gal4
D
V
Wg
C
ap>tkv+
D
V
Wg
dppZ
Wing
D
dppZ
E
ap>
D
V
Wg
dppZ
Haltere
F
dppZ
G
ap>tkvRNAi
D
V
Wg
dppZ
Haltere
H
dppZ

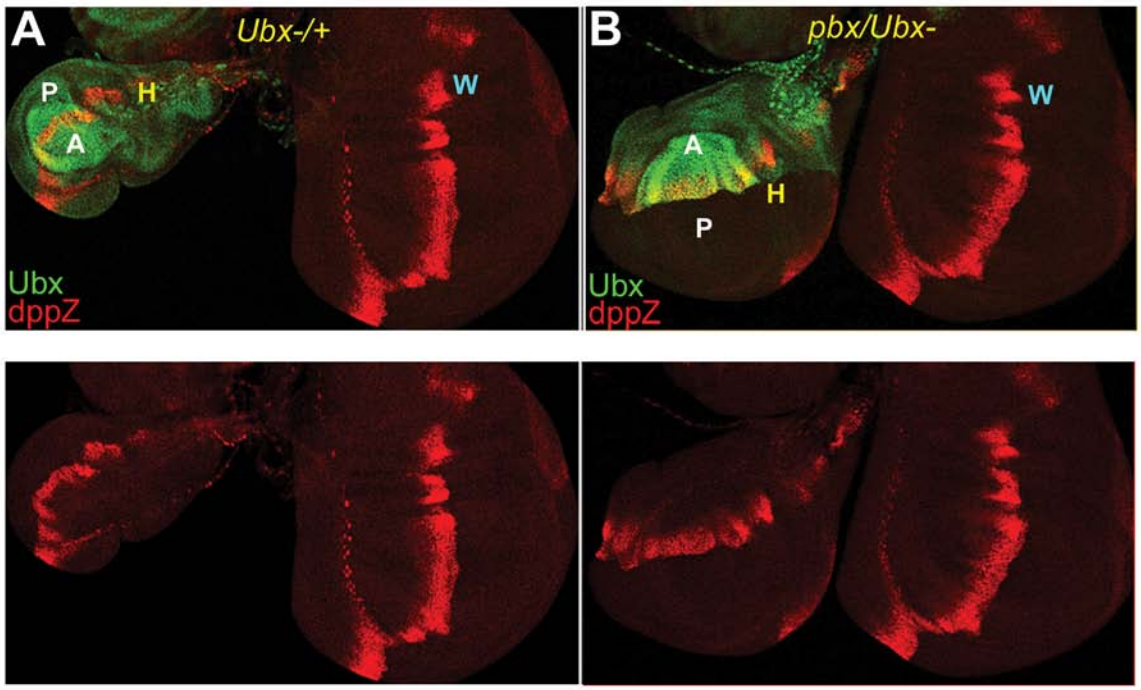
A
Ubx-/+
P
H
A
W
Ubx
dppZ
B
pbx/Ubx-
A
H
P
W
Ubx
dppZ